Delft University of Technology

Design of a Direct numerical Simulation of flow and heat transfer in a T-junction

Ajay Kumar, Aniketh; Mathur, Akshat; Gerritsma, Marc; Komen, Ed

Important note
To cite this publication, please use the final published version (if applicable).
Please check the document version above.

Design of a Direct numerical Simulation of flow and heat transfer in a T-junction

Aniketh Ajay Kumar [a,b], Akshat Mathur [a,*], Marc Gerritsma [b], Ed Komen [a]

[a] *Nuclear Research & Consultancy Group, 1755 LE Petten, the Netherlands*
[b] *Faculty of Aerospace Engineering, TU Delft, 2629 HS Delft, the Netherlands*

ARTICLE INFO

ABSTRACT

Several investigations have been undertaken to study the velocity and temperature fields associated with the thermal mixing between fluids, and resulting thermal striping in a T-junction. However, the available experimental databases are not sufficient to describe the involved physics in adequate detail, and, due to experimental limitations, accurate data on velocity and temperature fluctuations in regions close to the wall are not available. Computational Fluid Dynamics (CFD) can play an important role in predicting such complex flow features. However, predicting complex thermal fatigue phenomena is a challenge for the available momentum and heat flux turbulence models. Furthermore, such models need to be extensively validated.

The aim of the present work is to design a reference numerical experiment for Direct Numerical Simulation (DNS) of a thermal fatigue scenario using Reynolds-Averaged Navier-Stokes (RANS) simulations. First, the feasibility of scaling down the Reynolds number from experimental cases to a computationally-feasible range is investigated. The junction corner shape is also modified to a slightly rounded corner, ensuring that the underlying fundamental physical phenomena of turbulence and thermal mixing flow features are preserved. Finally, the pipe lengths of the model were calibrated to ensure there would be no interference of the upstream developing region and the outlet boundary conditions on the thermal mixing at the junction. A sample under-resolved DNS case, with unity and low-Prandtl number passive temperature scalars, with *iso*-temperature, *iso*-flux and mixed (Robin) wall boundary conditions, are presented. This proof-of-concept simulation contributes to the finalization of the set-up for fully-resolved DNS with respect to the computational grid size selection and transient characteristics.

1. Introduction

T-junction geometries are widely used components in the nuclear industry. The study of thermal mixing in a T-junction geometry remains an ongoing interest of researchers. Understanding and predicting the effects of thermal mixing which result in cyclical thermal stresses and ultimately thermal fatigue on the walls of T-junctions can lead to major advancements in the design of T-junction geometries, having significant positive implications on the maintenance and life of these cooling components. Numerous experiments and projects have been undertaken to study thermal mixing between the fluids and thermal striping/fatigue on the wall.

An experimental campaign on thermal mixing in water was undertaken at the Vattenfall facility (Westin et al. (Westin et al., 2006; Westin et al., 2008); Odemark et al. (Odemark et al., 2009) for a T-junction with branch-to-main inlet diameter ratios of 1:1.4–1.54. The inlet Reynolds number (based on inlet velocity and diameter) ranged between 8×10^4 – 8×10^5. Accompanying numerical simulations were also performed in order to validate modelling approaches. It was reported that Large Eddy Simulation (LES) and Detached Eddy Simulation (DES) approaches showed good qualitative comparison to the experimental data. However, the near-wall resolution was too coarse therein to accurately predict the thermal mixing in the T-junction. An OECD-NEA benchmark exercise was conducted in order to investigate the modelling capabilities based on this experimental dataset (Smith et al. (Smith et al., 2013). It was reported again that LES performed remarkably well in predicting temperature and velocity distribution.

The MOTHER project was another collaborative effort into studying the predictive accuracy of different turbulence modelling methods for water in a T-junction geometry, including conjugate heat transfer with

---

* Corresponding author.
E-mail address: mathur@nrg.eu (A. Mathur).

the solid walls. Braillard et al. (Braillard et al., 2018) reported experimental measurements performed at FATHERINO facility of CEA for both rounded and sharp corner geometries. Both sharp and rounded corner geometries were considered within the project, at two different inlet Reynolds numbers – 4×10^4 and 6×10^4. Shams et al. (Shams et al., 2018) reported a validation study with a total of 29 different CFD simulations, including LES, hybrid LES-RANS and (U)-RANS methodologies. It was reported that LES was the more accurate approach with its prediction of the flow and thermal fields. However, the computational costs also ramp-up rapidly with increasing Reynolds numbers. Additionally, long sampling time is required to attain a statistically converged solution for the accurate prediction of the temperature fields in the solid. For these reasons, LES is considered too expensive to be used as a predictive tool.

Kamide et al. (Kamide et al., 2009) reported the water experiments at the WATLON facility with branch-to-main inlet diameter ratio of 1:3. Within the collaborative ATLAS+ project, CFD was employed to reproduce the experimental measurement of transient temperature behavior at the wall (De Santis and Shams (De Santis and Shams, 2018). It was reported that k-ω SST turbulence model provides the best accuracy and stability of the solution within the RANS framework. However, the magnitude and frequency of temperature fluctuations were not accurately represented by RANS. A reasonable trade-off between computational effort and accuracy can be made using this turbulence model, since LES is too computationally demanding.

Howard and Serre (Howard and Serre, 2015) stated that RANS models relying on the Boussinesq eddy viscosity models are found to inadequately capture the flow physics in the T-junction geometry simulations due to their inability to model non-equilibrium turbulence. The non-equilibrium flows involved require the implementation of advanced wall functions to capture its effects. Similar conclusion was also reported for wall functions employed in wall-modelled LES (WM-LES) by Jayaraju et al. (Jayaraju et al., 2010). Frank et al. (Frank et al., 2010) noticed that the wall-function approaches systematically under-predict the fluctuations near the boundaries. This implies that resolving the small-scale structures in the near wall regions is crucial to accurately predicting the flow.

DNS of a planar T-junction with rectangular cross-section was recently presented by Georgiou and Papalexandris (Georgiou and Papalexandris, 2018). The important features involved in the flow including the large recirculation bubble and the separation zone formed at the junction region were reported. They concluded that the thermal mixing that is observed is a result of the shear layer between the mixing fluids, and additionally, the shear layer between the branch fluid jet and the recirculation bubble. The thermal mixing is also enhanced by the turbulence generated in the adverse pressure gradient regions downstream of the large recirculation bubble. This work also compared the performance of a wall-resolved LES and concluded that the LES faithfully reproduced the thermal mixing.

The above studies in the literature clearly indicate the need for numerical tools to faithfully predict the turbulent thermal mixing between the fluids, and thereby thermal fatigue/stripping in the solid walls. Before a validation exercise can be performed to further develop and calibrate the RANS modelling strategies, a high-quality reference database is needed. Thus, the objective of the present study is to design a high-resolution DNS case for thermal mixing in a T-junction. Although some recent works in the literature have reported high-fidelity numerical data for thermal mixing in T-junctions (Jayaraju et al., 2010; Frank et al., 2010; Georgiou and Papalexandris, 2018; Ung et al., 2014; Kang et al., 2019; Hattori et al., 2014), there still remains a gap with respect to DNS of circular pipe T-junction, which will be addressed herein. Past numerical studies have also reported only near-unity or high-Prandtl number flows. In the present DNS case, however, it is planned to incorporate both unity- and low-Prandtl number temperature scalars. The planned DNS may provide crucial data in understanding of turbulent heat transfer and thermal mixing mechanisms in T-junction

geometries, especially for low-Prandtl fluids such as liquid metals, experimental measurements for which are difficult to obtain and high-fidelity numerical data in the literature is scarce. The DNS case will also include mixed thermal boundary conditions (Robin) at the wall which is reported to mimic the conjugate heat transfer with the solid wall (Flageul et al., 2015), as discussed later. This novel addition to the DNS case will provide a realistic boundary condition, as opposed to *iso*-flux (Dirichlet) or *iso*-temperature (Neumann) conditions.

The undertaking of such extensive DNS campaign requires preparation. In that context, a preliminary design and calibration exercise is reported herein in order to set up a DNS case. Reference experimental datasets in the literature employ geometries comprising of sharp corners at significantly high Reynolds numbers, which are computationally too expensive to reproduce in a DNS calculation. Thus, the first step in this process is to identify the corner shape required in the geometry, followed by the scaling down of the Reynolds number to a more computationally feasible value for a DNS, without significant loss in fundamental flow features. This is followed by a geometry optimization procedure to reduce the size of the computational domain required. Based on the previous efforts reported in the literature, a steady-state RANS modelling strategy using the k-ω SST turbulence model is employed for calibration herein. The final case set up is employed to perform a proof-of-concept under-resolved DNS calculation, also reported herein. The objective of the under-resolved calculation, here, is to demonstrate the case set up and assess the feasibility of the fully-resolved DNS calculation. The UDNS results herein may also be used to finalize the meshing strategy implemented, along with any other simulation parameters of note.

2. RANS calibration of the T-junction

The RANS simulations are performed using the Siemens STAR-CCM+ v12 solver, using its implicit k–ω SST turbulence model. Second-order upwind differencing scheme is used for discretization of flow, temperature and turbulence parameters. The geometry used in the calibration of the T-junction problem is as shown in Fig. 1. The inlet and branch pipes are connected perpendicularly to each other and meet at the T-junction, where the mixing of the fluids from these pipes takes place and flow downstream through the outlet pipe. The corner of the junction can be prescribed with a radius of curvature. A diameter ratio of unity (i.e., ratio of diameters of branch to inlet pipe) is selected for the present case. The main inlet pipe serves as the cold fluid inlet, while the hot fluid is injected at the branch inlet. A Prandtl number of unity is set for thermal properties of the fluid.

2.1. Corner shape calibration

Sharp junction corners can present a stringent mesh requirement for a DNS calculation, increasing the total mesh size. Additionally, the small mesh elements at the corner may lead to high Courant numbers, resulting in smaller time-step size. Thus, to ease the computational effort for the DNS calculation, a calibration is first performed for the corner shape. Computations are performed using different corner radii ranging from $r_c/D = 0.02 - 0.33$. It should be noted that smaller values of corner radii resulted in significant increase in mesh sizes, and thus are not investigated here. It is observed that the corner radius of $r_c/D = 0.02 - 0.04$ resulted in a reasonable depiction of the phenomena observed in sharp corner geometry, as can be seen in Fig. 2 below. At higher radii of curvatures, the flow appears to exhibit transient features. Thus, a radius of $r_c/D = 0.02$ is selected for the case set up.

2.2. Reynolds scaling simulations

A significant issue with the available experimental datasets is that the Reynolds numbers are unreasonably high for reproducing the flow numerically. Thus, an investigation is performed to scale down the *Re*,
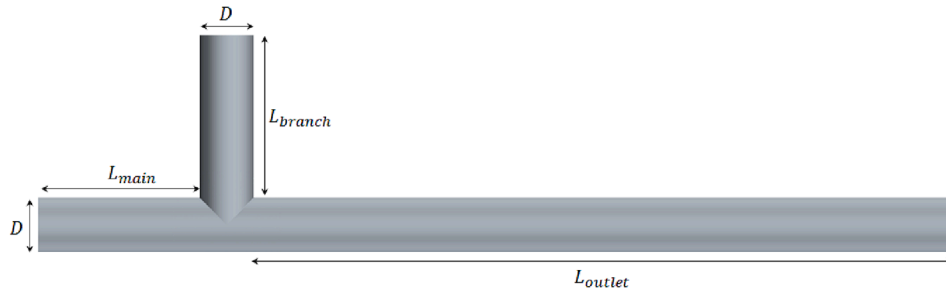
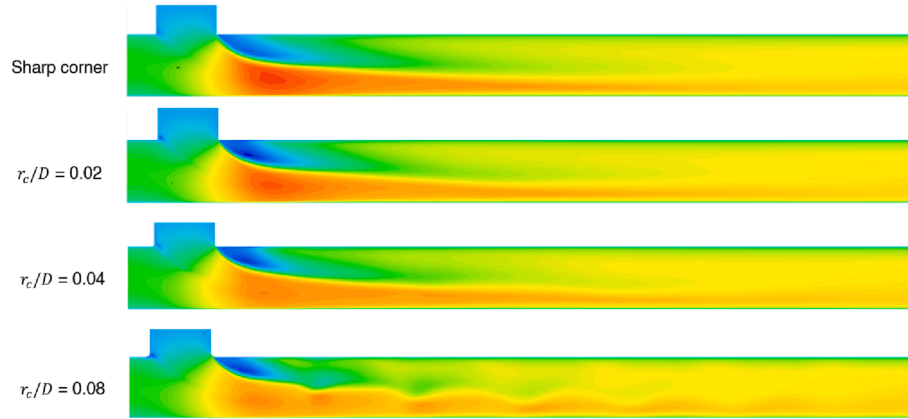**Fig. 1.** T-Junction geometry employed in the present study.

Fig. 2. Streamwise velocity contours for different corner radii.

ensuring that fundamental turbulence and thermal mixing flow features observed at higher *Re* are similar to those at lower, computationally-feasible *Re*. The scaling test of Reynolds numbers is carried out at values of $Re = 20000$, 40,000 and 60,000 (where Reynolds number, $Re = U_b D / \nu$, is based on bulk inlet velocity and pipe diameter), and at values of $Re = 5300$, 9100 and 11,700 (corresponding to friction
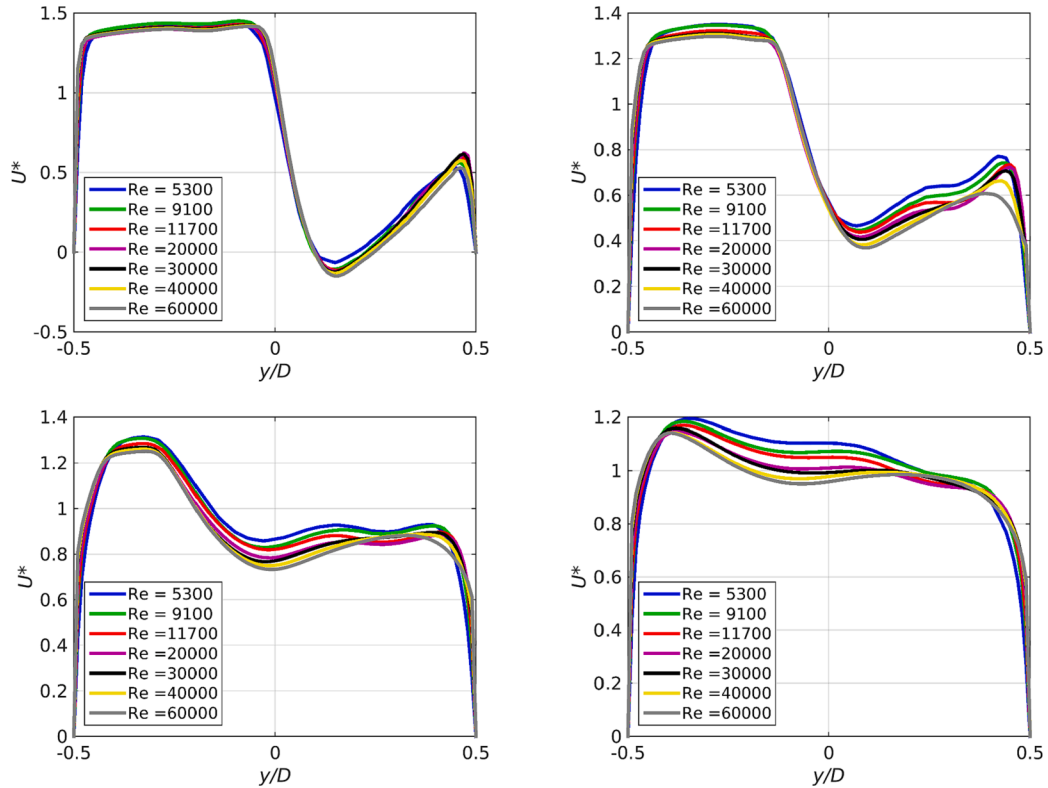

Fig. 3. Streamwise velocity profiles for different Reynolds numbers at (a) 1D, (b) 2D, (c) 4D and (d) 8D downstream of the junction.

Reynolds numbers of $Re_\tau = 180$, 290 and 360). Here, Reynolds numbers are based on diameter – $Re = U_b D/\nu$ and $Re_\tau = u_\tau D/\nu$.

Velocity and temperature profiles at locations 1D, 2D, 4D and 8D downstream of the junction are compared at different locations downstream of the T-junction, for the different Reynolds numbers studied herein, as shown in Figs. 3 and 4. Here, the velocity is normalized with the value of the bulk velocity at the outlet, as $U^* = U/U_b$, while the temperature is normalized between zero and unity, as $T^* = (T - T_{low})/(T_{high} - T_{low})$, where T_{high} and T_{low} are the fluid temperatures at the branch and main inlet pipes, respectively. There are marginal differences in both the flow and thermal fields in the upper region of the pipe. However, the overall physics of flow separation, recirculation and thermal mixing are also observed for all the Reynolds numbers studied herein. This implies that the scaling of the Reynolds number down to more feasible values for a DNS is possible. An inlet Reynolds number of $Re = 5300$ ($Re_\tau = 180$) is chosen for the present DNS case set up in order to reduce computational costs.

It is noted that variations in normalized turbulent kinetic energy profiles exist (not shown here for the sake of brevity) in the present range of Reynolds numbers. Those differences, however, may be attributed to the performance of the turbulence model itself for different Reynolds number flows, especially when the lowest Reynolds number here ($Re_\tau = 180$) is close to the lower limit of turbulent flow regime. For this reason, turbulent kinetic energy profiles are not studied in further detail to determine the scalability of Reynolds numbers. Moreover, the mean flow and thermal mixing characteristics predicted by the turbulence model shows a remarkable scalability for all Reynolds numbers here.

2.3. Pipe length optimization

Further, an optimization study on pipe lengths is performed on the T-junction geometry. For the two inlet pipes, it is ensured that the flow development from the inlet region is not affected by the thermal mixing

in the junction. This is done by checking how far upstream from the junction do the flow parameters deviate from fully-developed profiles. For this, simulations are performed with upstream lengths of 6D in both main and branch inlets. It should be noted that an additional length of recirculating regions is included in each inlet, ensuring flow development. Fig. 5(a) and (b) show the integral percentage difference in the flow parameters at different upstream locations from the junction for the main and the branch inlet respectively, with reference to fully-developed pipe flow profiles. It is seen from the error estimates that an upstream length of 2D is sufficient to eliminate effect of thermal mixing on both main and branch inlets. However, an additional length of 1D is included as a safety margin. Thus, the total inlet lengths upstream of the junction is set at 3D.

The length of the outlet pipe is finalized based on how far upstream does the outlet boundary condition (BC) affect the turbulent mixing in the region of interest (i.e. up to 8D downstream of the junction). Separate simulations are performed with total outlet pipe lengths of 8D, 10D, 12D, 14D and 16D. Comparisons are made for flow profiles from simulations with outlet lengths 8D, 10D, 12D and 14D with those from the simulation with an outlet length of 16D. It is seen that the change in downstream flow parameters for all outlet lengths, with respect to the reference 16D outlet length, are sufficiently low except for that in 8D outlet length. This is expected as the outlet BC at 8D is bound to affect the flow profiles in the vicinity (which lies in the region of interest). Hence to avoid all effects of the boundary, an outlet length of 12D is selected. The integral percentage difference in flow parameters at different downstream locations for the outlet pipe length of 12D, with respect to the reference outlet pipe length, is illustrated in Fig. 6. A safety margin of 1D is also included, making the final length of the outlet pipe as 13D.

2.4. RANS meshing strategy

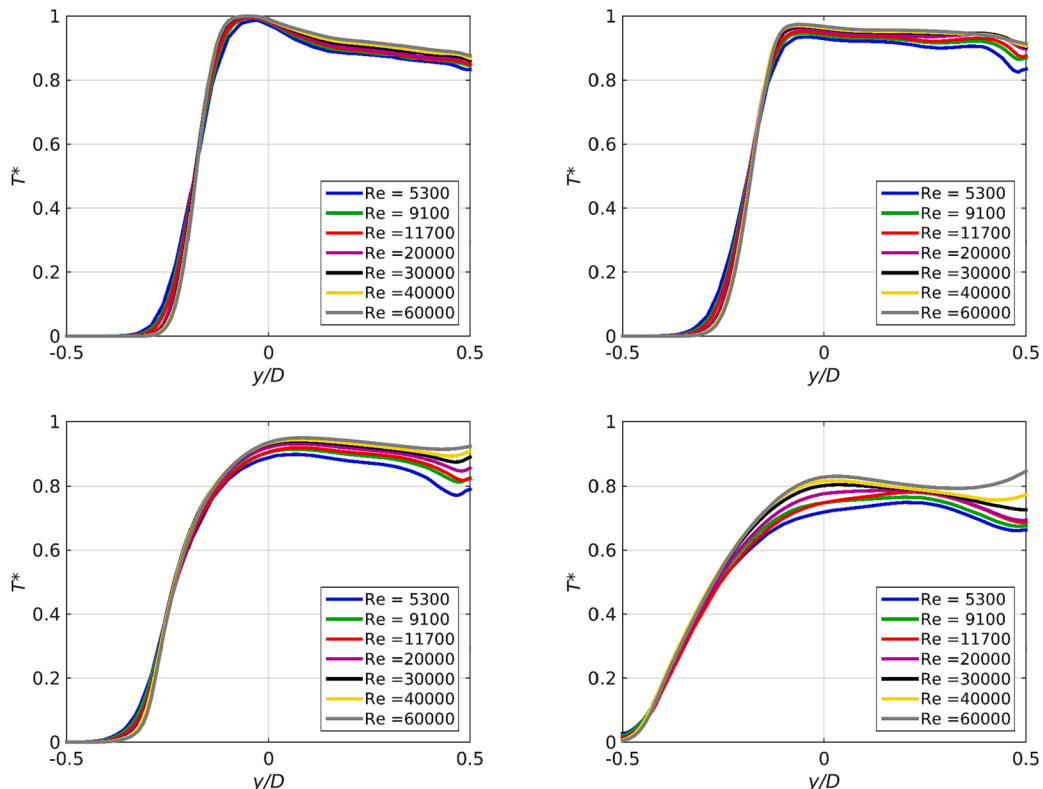The geometry is mapped with polyhedral cells in the junction, while

Fig. 4. Normalized temperature profiles for different Reynolds numbers at (a) 1D, (b) 2D, (c) 4D and (d) 8D downstream of the junction.
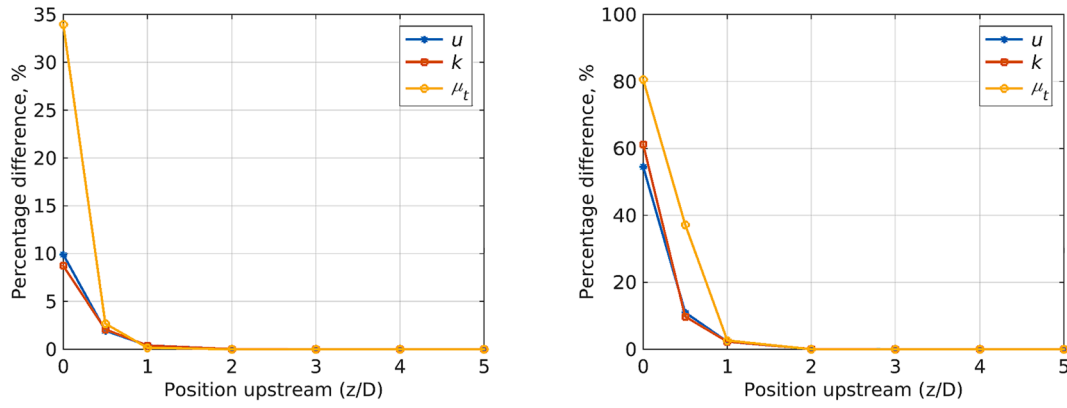
Fig. 5. Percentage difference in different upstream profiles for the two inlet pipes.
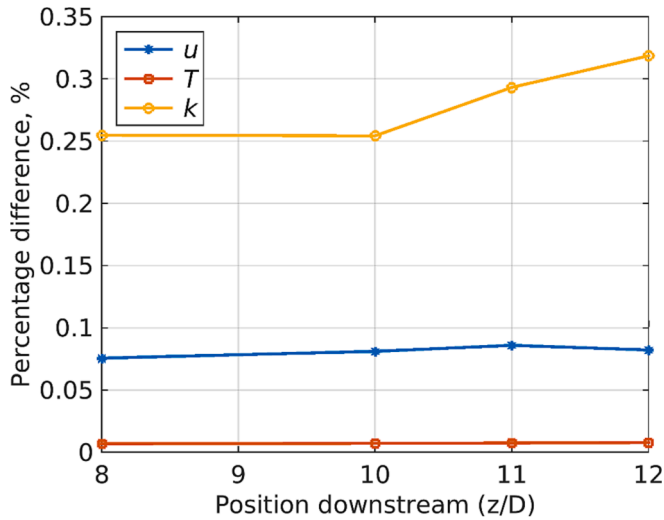

Fig. 6. Percentage difference in different downstream profiles for the outlet pipe.

Fig. 7. Mesh on the T-junction cross-section for inlet $Re_\tau = 180$.

the mesh is extruded from the junction in each inlet and outlet legs. Prism layers are used in the entire geometry to resolve the flow up to the wall. An iterative meshing strategy is adopted for the RANS simulations whereby a mesh sensitivity is performed after each of the above calibration steps. It is ensured that all results presented herein are grid independent, and that the normalized grid parameters (i.e. y^+_{wall}, Δy^+_{bulk}, Δz^+, etc.) are similar for each simulation. The surface-average y^+_{wall} in the entire geometry is kept below 0.4, while the maximum value at the junction rounded corners is roughly 2.0. A snapshot of the mesh on the junction cross-section for inlet friction Reynolds number, Re_τ, equal to 180 and rounded corners ($r_c/D = 0.02$) is illustrated in Fig. 7.

3. Mixed (Robin) boundary condition

Inclusion of conjugate heat transfer (CHT) with solid walls in DNS amounts to large computational costs due to the slow statistical convergence of the thermal fields in the solid region. Flageul et al. (Flageul et al., 2015) has shown that a mixed (Robin) wall BC is able to sufficiently mimic CHT wall BC. A mixed BC may be represented by,

$$AT + B\partial_y T = C \tag{1}$$

where A, B and C are coefficients. With manipulations (Flageul et al. (Flageul et al., 2015), it can be obtained,

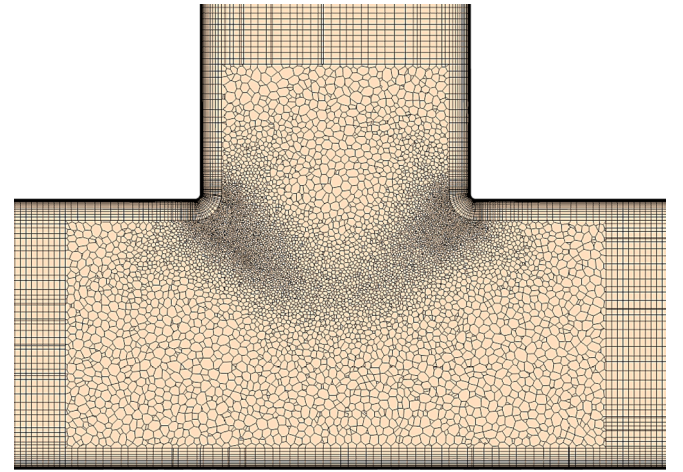$$A^2/B^2 = \langle T'^2 \rangle / \langle \partial_y T' \partial_y T' \rangle \tag{2}$$

Here, the numerator represents the temperature variance at the wall and the denominator represents its wall-normal component of dissipation. The former may be obtained from an *iso*-flux wall BC, and the latter from an *iso*-temperature wall BC, in separate calculations. Thus, parameter set (A, B) can be chosen for this modelling strategy. It should be noted that statistics of the fluctuating temperature are not directly influenced by coefficient C. The mixed BC showed closeness in statistics such as the turbulent heat fluxes, temperature variance and their budgets compared to the conjugate heat transfer (Flageul et al. (Flageul et al., 2015). Hence it is expected that a similar mixed BC approach in a T-junction geometry will sufficiently represent the CHT wall BCs.

In order to select the parameter set in the present calculation, separate channel flow DNS calculations at $Re_\tau = 180$ were performed with *iso*-flux and *iso*-temperature BCs (not presented here for the sake of brevity). It is estimated that ratio A^2/B^2 is equal to approximately 612.4 and 27.3 for Prandtl numbers 1 and 0.025, respectively. The value of coefficient B is kept equal to the thermal conductivity of the scalar, k ($= \mu C_p/Pr$).

4. Under-Resolved DNS calculation

4.1. Case Set-up

An under-resolved DNS (UDNS) calculation is performed to demonstrate the case set up. Simulation is performed using the spectral-element code Nek5000 (Fischer, xxxx). Nek5000 employs the Gauss-Lobatto-Legendre (GLL) polynomial expansion along each spatial direction. The velocity and the pressure fields are represented by the same

polynomial degree spatial discretization (the so-called P_N-P_N formulation). In order to avoid spurious pressure modes of the pressure–velocity collocated scheme, Nek5000 employs a high-order splitting approach (Tomboulides et al. (Tomboulides et al., 1997) that has shown high order accuracy in time and minimal mass conservation errors. The code offers a method of characteristics (OIFS) for time-advancement scheme whereby the calculations can run at CFL numbers higher than unity without loss in accuracy (Maday et al. (Maday et al., 1990); Fischer, xxxx). The present UDNS utilizes this scheme in third-order accuracy to keep CFL $\leq$ 2, which corresponds to a non-dimensional time-step of Δt^+ $\sim$ 0.006 (where $\Delta t^+ = \Delta t u_\tau^2 / \nu$).

As stated previously, an inlet Reynolds number of $Re = 5300$ ($Re_\tau =$ 180) is chosen for the present DNS case set up. The inlet and branch pipe lengths are 8D in length, which include a length of 5D recirculating region (Komen et al. (Komen et al., 2014). An outlet length of 13D is selected. The outflow is modelled with a turbulent outflow BC, while the walls are modelled as no-slip. Six temperature (passive) scalars are included as passive scalars in the calculation. The six scalars model *iso*-temperature (Dirichlet BC), *iso*-flux (Neumann BC) and mixed wall conditions (Robin BC), each for a Prandtl number of 1.0 and 0.025. The results of the calibration study summarized above form the basis of the case setup of the UDNS case. The wall friction and Kolmogorov length scale estimates from RANS determine the mesh requirements for the bulk and near-wall regions. It should be noted that the present meshing strategy (which is based on the estimates for the mixing region) maps the cross-section with the same number and size of cells in both the inlet and outlet regions. Further discussion on the spatial resolution in these regions is presented later.

The domain is mapped with a macro-element grid size of 270480, which meets the fully-resolved DNS requirements at a spatial discretization of polynomial order of N = 9. However, the present UDNS is performed at a polynomial order of N = 3. This gives a total of 17.3×10^6 GLL grid points for the present UDNS. The discretization across the pipe cross-section is illustrated in Fig. 8. At this discretization, the maximum wall y^+ in the inlet, outlet and junction regions are estimated to be 0.7, 1.5 and 5.7, respectively. The radial resolution in the bulk is estimated to be roughly 13.5 wall units.
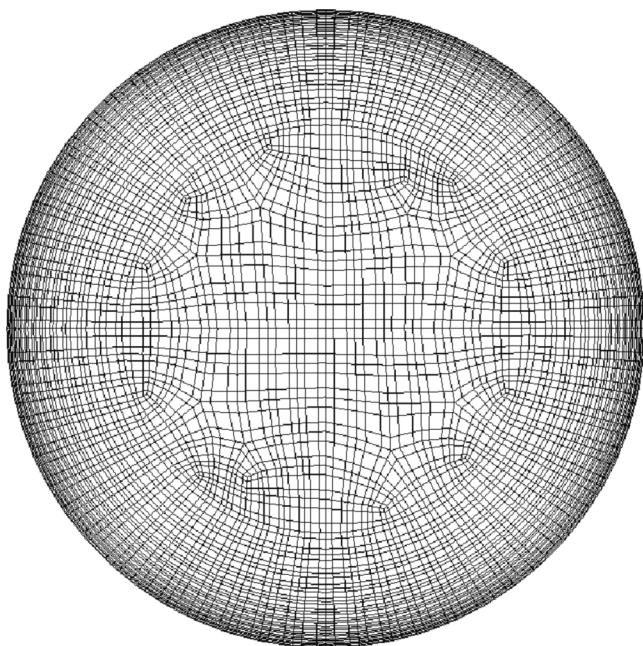

Fig. 8. Mesh on the pipe cross-section discretized at N = 3 polynomial order.

4.2. UDNS results

Fig. 9(a) presents the wall friction velocity history plot for the inlet, branch and outlet legs and Fig. 9(b) presents the integral wall heat flux history plot of the two *iso*-temperature scalars. The flow transient is observed to be characterized by an initial period of flow development, followed by a quasi-steady state. In the present UDNS, the statistical calculation is started at $t^* = 100$, after the flow reached a fully-developed state (where $\Delta t^* = t U_b / D$, and U_b is the bulk velocity of the inlet). The calculation is performed for several time-averaging periods as indicated in Fig. 9(b), and the statistical convergence is estimated by comparing the change in velocity and temperature statistics at downstream locations of the T-junction. The change in the mean and r.m.s. fluctuating quantities at different averaging periods with respect to those at the final averaging period of $\Delta t_1^* = 400$ (or $\Delta t_1^+ \sim 2500$) is illustrated in Fig. 10 (a) and (b), respectively. The percentage change in statistical quantities is averaged over several sampling lines in the region 0 – 10D downstream of the T-junction. In the figure, the horizontal axis represents the difference in time-averaging periods, with respect to the final averaging period of $\Delta t_1^* = 400$. It is seen that change in mean and r.m.s. quantities at the last sampled averaging period is less than 0.5% with respect to those at Δt_1^*. This is considered to be sufficiently converged. Thus, the results presented hereafter correspond to time-averaging period of $\Delta t_1^* = 400$. It should be noted that higher-order statistics are not assessed here, as the low spatial resolution is likely to result in these statistics not converging at all.

The statistical quantities for the present UDNS calculation are presented next. It should be noted that all quantities are qualitatively discussed, as any quantitative analyses of under-resolved calculation is less significant. The contour plots of instantaneous and time-averaged mean velocity magnitude are presented in Fig. 11(a) and (b), respectively. The axial and radial time-averaged r.m.s. components of velocity are presented in Fig. 12(a) and (b), respectively. The plots clearly show the well-defined flow separation region immediately downstream of the junction at the upper wall, characterized by the low values of mean streamwise velocity corresponding to the region of high magnitude of the r.m.s. quantities. The higher mean values of the streamwise velocity below this region are representative of the mixing of the flows in the center of the pipe. It is observed that there is pixelation in the r.m.s. contours of the results of this UDNS case. This is likely due to physics not being captured due to the inadequate resolution offered by the present spatial discretization of the lower polynomial order.

The instantaneous, mean and r.m.s. fluctuating component of the temperature scalars are presented in Figs. 13, 14 and 15, respectively. Following the velocity contours, a clear mixing region can be seen in the middle of the pipe downstream of the T-junction. There is a stark contrast between the contours of the different Prandtl number scalars. The Prandtl number being the ratio of the momentum diffusivity to the thermal diffusivity of the fluid concerned, implies that a lower value would show an increased diffusion of temperature through the same flow field. This can be clearly observed in the contour plots – the unity Prandtl number scalars show a larger region with higher temperature values at the top half of pipe; whereas in the low-Prandtl number scalars, the temperature appears to have diffused very close to the start of the mixing at the junction. The r.m.s. contours of the unity Prandtl number scalars further validate that the spatial discretization used needs to be further resolved to capture the physics of the thermal field.

As stated previously, the coefficients of the mixed BC are estimated from separate channel flow DNS simulations at $Re_\tau = 180$ in order to mimic the condition of CHT. The fluctuating component of the temperature scalars are affected directly by the BC coefficients. Thus, it is expected that only the r.m.s. fluctuating component of these scalars mimic the CHT condition. On the other hand, the absolute value of the scalar has little significance here. Fig. 16 presents the contour plots of the r.m.s. fluctuating component of these scalars.
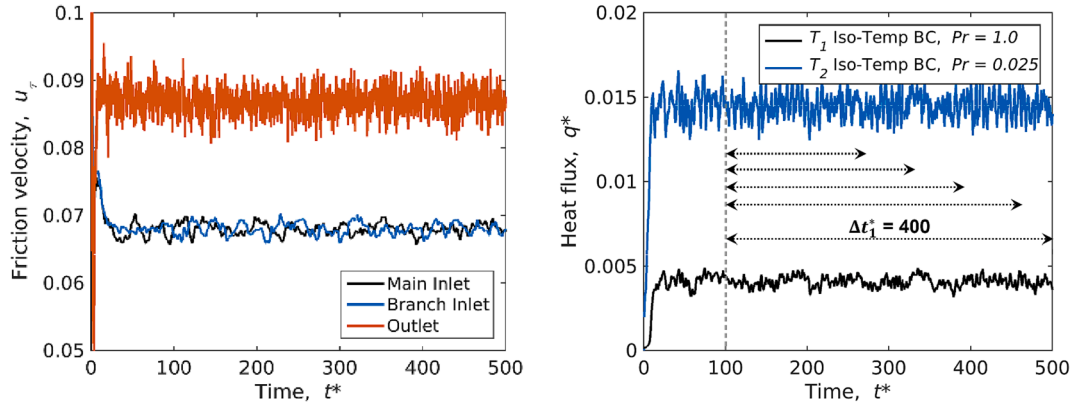
Fig. 9. (a) Wall friction velocity history plot for the inlet and outlet pipes, and (b) wall heat flux history plots for the two *iso*-temperature scalars. Also shown in (b) are the different time-averaging periods employed in the estimating statistical convergence.
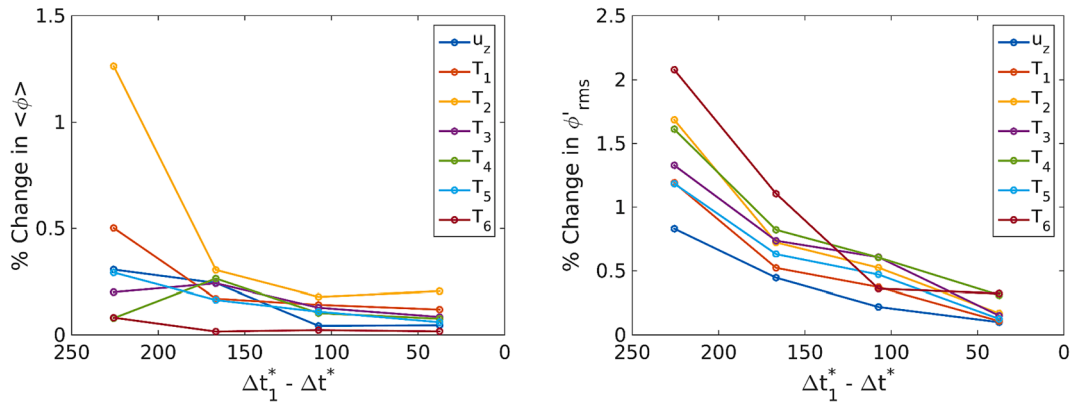

Fig. 10. Percentage change in statistics between different averaging periods with respect to Δt_1^* ($=400$) for (a) mean, and (b) r.m.s. fluctuating quantities.
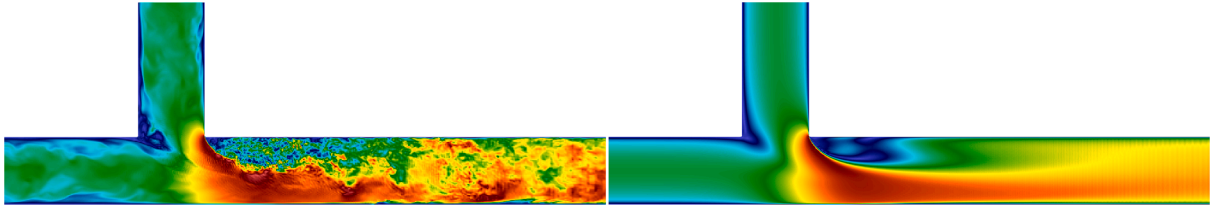

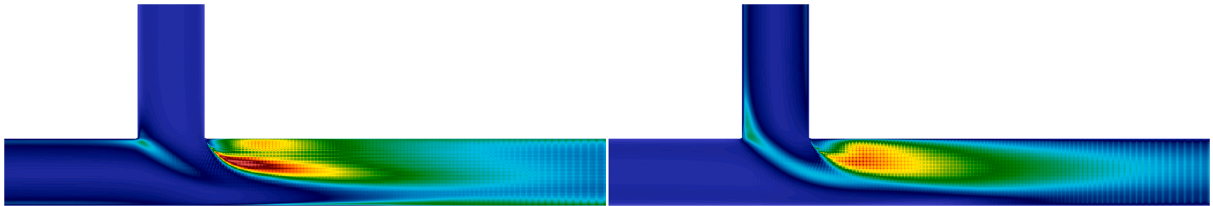**Fig. 11.** (a) Instantaneous and (b) mean velocity magnitude.

Fig. 12. R.M.S. of fluctuating velocity for (a) axial and (b) radial velocity.

The estimates for the mesh requirements for the final DNS are re-assessed using the present UDNS results. The recommended cell size for fully resolving physics of turbulent flow is $\Delta = \pi \eta_k$ (Pope (Pope, 2000). The estimated Kolmogorov length-scales for the present results are calculated from the dissipation of turbulent kinetic energy as $\eta_k = \left(\nu^3/\varepsilon \right)^{1/4}$, where ν and ε are the kinematic viscosity and turbulent kinetic energy dissipation, respectively. Fig. 17 presents the local spatial

discretization, $\Delta = \left(\Delta x \Delta y \Delta z \right)^{1/3}$, normalized by η_k. It is seen that the maximum value of this quantity reaches ~ 13 in the mixing zone. Interpolating from the present discretization, polynomial order of $N = 9$ should reduce this value to roughly ~ 4, which can be considered to be fully-resolving discretization. However, this value is expected to reduce to less than 1 in the upstream inlet regions and to ~ 2 in the downstream outlet region. This is an unnecessary 'over-resolution' of those regions
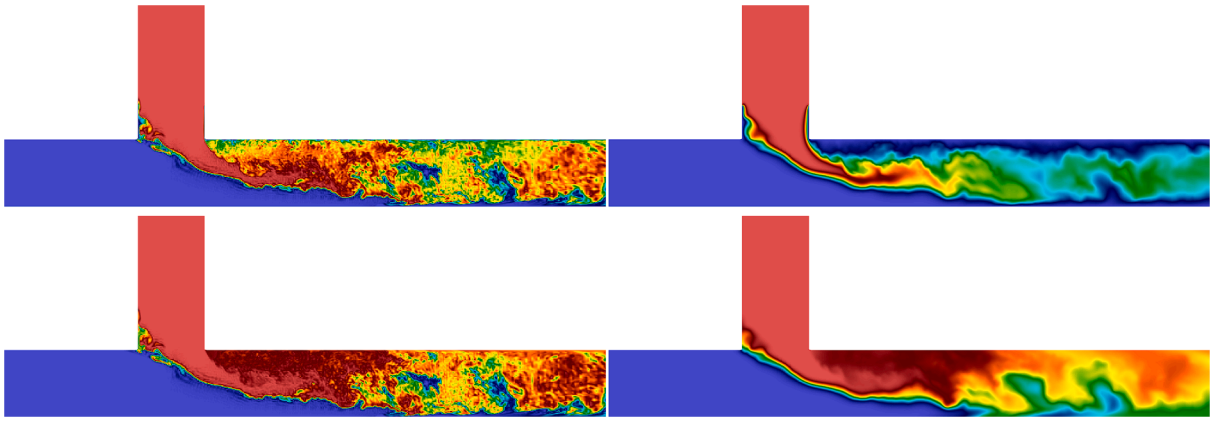
Fig. 13. Instantaneous temperature scalars (a) *iso*-temperature BC, Pr = 1; (b) *iso*-temperature BC, Pr = 0.025; (c) *iso*-flux BC, Pr = 1; (d) *iso*-flux BC, Pr = 0.025.

Fig. 14. Mean of temperature scalars (a) *iso*-temperature BC, Pr = 1; (b) *iso*-temperature BC, Pr = 0.025; (c) *iso*-flux BC, Pr = 1; (d) *iso*-flux BC, Pr = 0.025.

Fig. 15. R.M.S. fluctuations of temperature scalars (a) *iso*-temperature BC, Pr = 1; (b) *iso*-temperature BC, Pr = 0.025; (c) *iso*-flux BC, Pr = 1; (d) *iso*-flux BC, Pr = 0.025.
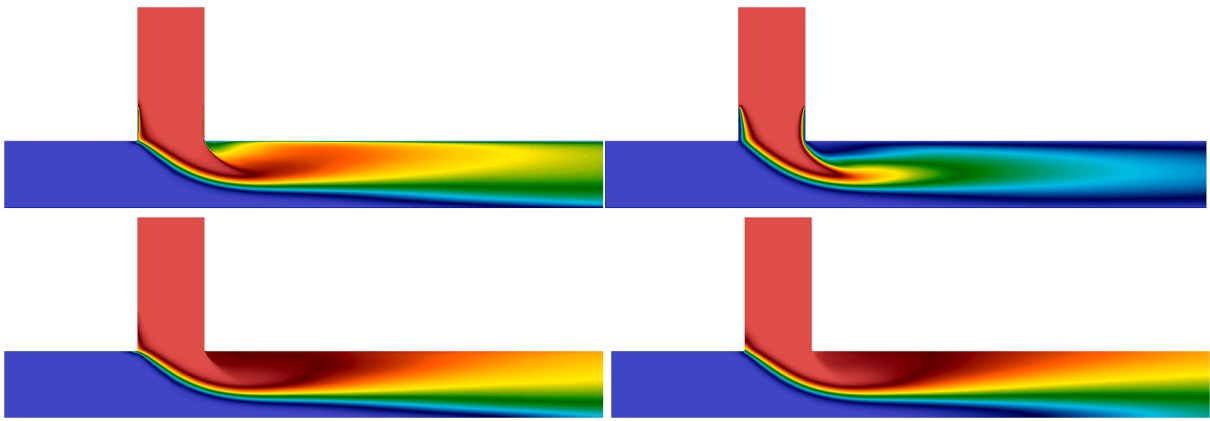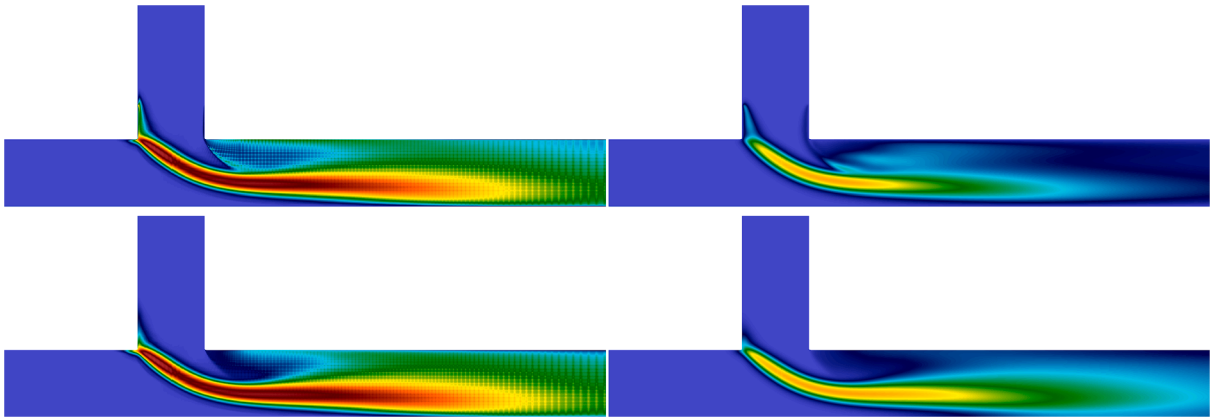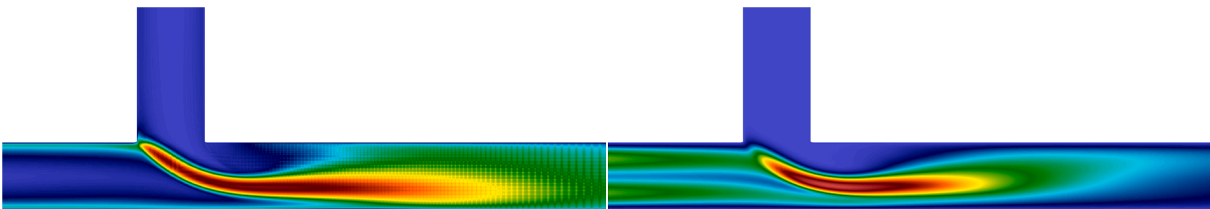

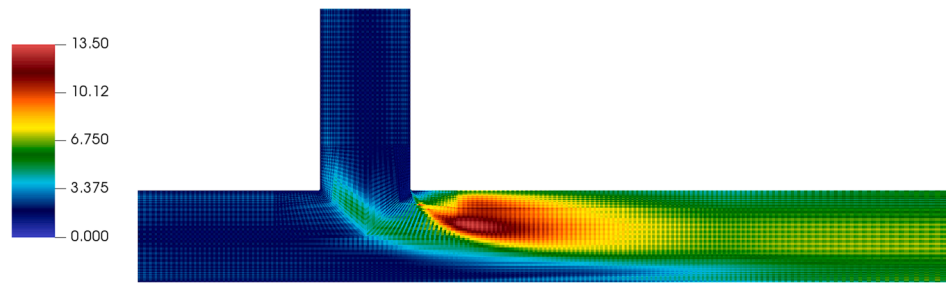**Fig. 16.** R.M.S. fluctuations of mixed BC temperature scalars, (a) Pr = 1, and (b) Pr = 0.025.

Fig. 17. Cell size normalized by Kolmogorov length-scale (Δ/η_k).

compared to the local flow physics. It is recommended that a different meshing strategy be investigated whereby different number of cells and cell sizes can be mapped across the cross-section along the length of a pipe. With this strategy, the macro-element distribution may be adapted to the local flow requirements, in order to save computational requirement of the final DNS.

Further, the distribution of CFL numbers based on local instantaneous velocities is presented in Fig. 18. Also shown in the plot is the mesh discretization at the polynomial order of N = 3. As stated previously, time-stepping in the present calculation is regulated by a maximum CFL of 2. It is seen that this maximum value appears in only a few cells at the junction corner. The maximum allowed time-step appears to be limited due to only these few cells. Thus, a further optimization of the mesh is also recommended for the final DNS in order to ease this bottle-neck condition.

5. Conclusions

The calibration of a T-junction geometry for a DNS calculation is undertaken using RANS CFD simulations. The corner shape of the T-junction is modified to a corner with a radius of curvature, $r_c/D = 0.02$ so as to reduce computational costs of a sharp corner. A Reynolds scaling study is then performed to ensure the fundamental flow phenomena observed at higher Reynolds numbers are reproduced at lower, computationally-feasible Reynolds numbers. A Reynolds number of $Re = 5300$ ($Re_\tau = 180$) is finalized for the UDNS computation. A pipe length optimization study is then conducted to minimize the computational domain of the T-junction and therefore lower the computational cost of the UDNS. This results in fixing the inlet and branch lengths each at 8D (with the recirculating regions), and the outlet length at 13D (including a margin of safety). The inferences of the RANS calibration study are then used to set-up and run an under-resolved DNS calculation for the T-junction geometry. The time-averaging statistical calculations were started after a fully-developed flow was attained. It is shown that the statistics up to second order are sufficiently converged herein. The contours of the instantaneous, mean, and r.m.s. of velocity, along with those of the several temperature scalars have also been presented.

The results of the present UDNS may be utilized to finalize the final DNS. The transient characteristics of the calculation provides a good estimate for the time period required for the flow to fully-develop in the domain. This provides the time at which time-averaging can be started in the calculation. The UDNS also provides a better estimate of the Kolmogorov length-scales, which can be used to assess the grid size requirement for a fully-resolved DNS. The present results for the polynomial order of N = 3 confirm the same from preliminary RANS that the present mesh will achieve the fully-resolved criteria for DNS at a polynomial order of N = 9. This will result in roughly 270×10^6 GLL points. An estimate of the total time required for statistical convergence of time-averaged quantities is provided here as well. For the present results at N = 3, the time-averaged quantities show a statistical error of less than 1% for a time-averaging period of $\Delta t^* \sim 400$.

Further optimizations of the meshing strategy may be performed for the upstream and downstream regions from the junction, as the present
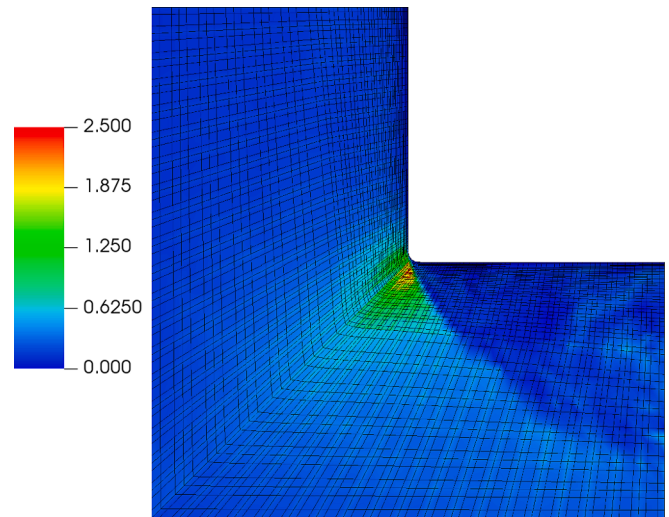

Fig. 18. Instantaneous distribution of CFL numbers at the junction corner.

strategy results in an unnecessarily high resolution in those regions. However, reduction in computational costs are not expected to be significantly large. The mesh at the junction corner is also recommended to be optimized to ease the CFL requirement for the cells in the corner. This can greatly affect the time-stepping, reducing the overall computational costs. Finally, it is recommended to analyse the results for the mixed BC in detail, in order to see assess the capability and limitation of this condition.

CRediT authorship contribution statement

Aniketh Ajay Kumar: Methodology, Validation, Investigation, Visualization, Writing – original draft. **Akshat Mathur:** Conceptualization, Methodology, Visualization, Writing – original draft, Supervision. **Marc Gerritsma:** Conceptualization, Methodology, Writing – review & editing, Supervision. **Ed Komen:** Conceptualization, Writing – review & editing, Supervision.

Declaration of Competing Interest

The authors declare that they have no known competing financial interests or personal relationships that could have appeared to influence the work reported in this paper.

Data availability

Data will be made available on request.

References

Braillard, O., Howard, R., Angele, K., Shams, A., Edh, N., 2018. Thermal mixing in a T-junction: Novel CFD-grade measurements of the fluctuating temperature in the solid wall. Nuclear Engineering and Design 330, 377–390. https://doi.org/10.1016/j.nucengdes.2018.02.020.

De Santis, A., Shams, A., 2018. Assessment of different URANS models for the prediction of the unsteady thermal mixing in a T-junction. Annals of Nuclear Energy 121, 501–512. https://doi.org/10.1016/j.anucene.2018.08.002.

Fischer, P. (n.d.). Implementation considerations for the OIFS/characteristics approach to convection problems. Retrieved from https://www.mcs.anl.gov/~fischer/Nek5000/oifs.pdf.

Fischer, P. (n.d.). NEK - fast high-order scalable CFD. Retrieved from https://nek5000.mcs.anl.gov/community/.

Flageul, C., Benhamadouche, S., Lamballais, É., Laurence, D., 2015. DNS of turbulent channel flow with conjugate heat transfer: Effect of thermal boundary conditions on the second moments and budgets. International Journal of Heat and Fluid Flow 55, 34–44. https://doi.org/10.1016/j.ijheatfluidflow.2015.07.009.

Frank, T.h., Lifante, C., Prasser, H.-M., Menter, F., 2010. Simulation of turbulent and thermal mixing in T-junctions using URANS and scale-resolving turbulence models in ANSYS CFX. Nuclear Engineering and Design 240 (9), 2313–2328. https://doi.org/10.1016/j.nucengdes.2009.11.008.

Georgiou, M., Papalexandris, M.V., 2018. Direct numerical simulation of turbulent heat transfer in a T-junction. Journal of Fluid Mechanics 845, 581–614. https://doi.org/10.1017/jfm.2018.256.

Hattori, H., Iwase, M., Houra, T., & Tagawa, M. (2014). DNS and LES for Turbulent Heat Transfer and Mixing in T-Junction Channel Flow. Presented at the 10th International ERCOFTAC Symposium on Engineering Turbulence Modelling and Measurements, Marbella, Spain.

Howard, R.J.A., Serre, E., 2015. Large-eddy simulation in a mixing tee junction: High-order turbulent statistics analysis. International Journal of Heat and Fluid Flow 51, 65–77. https://doi.org/10.1016/j.ijheatfluidflow.2014.11.009.

Jayaraju, S.T., Komen, E.M.J., Baglietto, E., 2010. Suitability of wall-functions in Large Eddy Simulation for thermal fatigue in a T-junction. Nuclear Engineering and Design 240 (10), 2544–2554. https://doi.org/10.1016/j.nucengdes.2010.05.026.

Kamide, H., Igarashi, M., Kawashima, S., Kimura, N., Hayashi, K., 2009. Study on mixing behavior in a tee piping and numerical analyses for evaluation of thermal striping. Nuclear Engineering and Design 239 (1), 58–67. https://doi.org/10.1016/j.nucengdes.2008.09.005.

Kang, D.G., Na, H., Lee, C.Y., 2019. Detached eddy simulation of turbulent and thermal mixing in a T-junction. Annals of Nuclear Energy 124, 245–256. https://doi.org/10.1016/j.anucene.2018.10.006.

Komen, E.M.J., Shams, A., Camilo, L.H., Koren, B., 2014. Quasi-DNS capabilities of OpenFOAM for different mesh types. Computers & Fluids 96, 87–104.

Maday, Y., Patera, A.T., Rønquist, E.M., 1990. An Operator-integration-factor splitting method for time-dependent problems: Application to incompressible fluid flow. Journal of Scientific Computing 5 (4), 263–292. https://doi.org/10.1007/BF01063118.

Odemark, Y., Green, T. M., Angele, K., Westin, J., Alavyoon, F., & Lundström, S. (2009). High-Cycle Thermal Fatigue in Mixing Tees: New Large-Eddy Simulations Validated Against New Data Obtained by PIV in the Vattenfall Experiment. In *Volume 3: Thermal Hydraulics; Current Advanced Reactors: Plant Design, Construction, Workforce and Public Acceptance* (pp. 775–785). Presented at the 17th International Conference on Nuclear Engineering, Brussels, Belgium: ASMEDC. https://doi.org/10.1115/ICONE17-75962.

Pope, S. B. (2000). *Turbulent Flows* (1st ed.). Cambridge University Press. https://doi.org/10.1017/CBO9780511840531.

Shams, A., Edh, N., Angele, K., Veber, P., Howard, R., Braillard, O., Niceno, B., 2018. Synthesis of a CFD benchmarking exercise for a T-junction with wall. Nuclear Engineering and Design 330, 199–216. https://doi.org/10.1016/j.nucengdes.2018.01.049.

Smith, B.L., Mahaffy, J.H., Angele, K., 2013. A CFD benchmarking exercise based on flow mixing in a T-junction. Nuclear Engineering and Design 264, 80–88. https://doi.org/10.1016/j.nucengdes.2013.02.030.

Tombouldies, A.G., Lee, J.C.Y., Orszag, S.A., 1997. Numerical simulation of low Mach number reactive flows. Journal of Scientific Computing 12 (2), 139–167. https://doi.org/10.1023/A:1025669715376.

Ung, H., Gilbert, D., Piller, O., Mortazavi, I., Iollo, A., 2014. LES and DNS Simulations of Imperfect Mixing for Double-tee Junctions. Procedia Engineering 89, 1268–1275. https://doi.org/10.1016/j.proeng.2014.11.434.

Westin, J., Alavyoon, F., Andersson, L., & Veber, P. (2006). Experiments and unsteady CFD-calculations of thermal mixing in a T-junction. In *Proc. Benchmarking of CFD Codes for Application to Nuclear Reactor Safety*. Presented at the CFD4NRS, Garching, Germany.

Westin, J., Veber, P., Andersson, L., 't Mannetje, C., Andersson, U., Eriksson, J., … Andersson, C. (2008). High-cycle thermal fatigue in mixing tees: Large-Eddy Simulations compared to a new validation experiment. In *Proceedings of the 16th International Conference on Nuclear Engineering*. Presented at the 16th International Conference on Nuclear Engineering, Orlando, USA.